Functional consequences of animal-to-animal variation in circuit parameters

Jean-Marc Goaillard[1,3], Adam L Taylor[1], David J Schulz[2] & Eve Marder[1]

How different are the neuronal circuits for a given behavior across individual animals? To address this question, we measured multiple cellular and synaptic parameters in individual preparations to see how they correlated with circuit function, using neurons and synapses in the pyloric circuit of the stomatogastric ganglion of the crab *Cancer borealis*. There was considerable preparation-to-preparation variability in the strength of two identified synapses, in the amplitude of a modulator-evoked current and in the expression of six ion channel genes. Nonetheless, we found strong correlations across preparations among these parameters and attributes of circuit performance. These data illustrate the importance of making multidimensional measurements from single preparations for understanding how variability in circuit output is related to the variability of multiple circuit parameters.

How tightly tuned do synaptic strengths and intrinsic membrane conductances need to be for a neuronal circuit to perform adequately? Theoretical work has shown that similar circuit performance can result from appreciably different sets of synaptic strengths and ionic conductance densities[1–4]. These studies suggest that if one were to look across a population of healthy adult animals, one might find substantial variability in synaptic strength and ion channel number, even in the same identified neuron. Moreover, recent experimental studies have found that membrane currents and synaptic strengths can vary several-fold across individual neurons of the same cell type[2,5–9]. In addition, there can be significant correlations between the conductances of voltage-gated currents[10] and between the genes that code for different channels[7,11].

How does variability in cellular and synaptic parameters relate to variability at the level of circuit function? We approached this question by measuring multiple cellular/synaptic parameters in each preparation to see how they correlated with circuit function, using neurons and synapses in the pyloric circuit of the stomatogastric ganglion (STG) of the crab *Cancer borealis*[12]. Some of these results might have been predicted from our current understanding of how the pyloric circuit works[13–15], but others are counterintuitive. Our results make clear the importance of collecting as much data as possible on individual preparations, rather than relying on studies of circuit parameters measured one-by-one in separate experiments.

RESULTS

The pyloric circuit (**Supplementary Fig. 1**) generates a rhythmic pattern of activity that drives contractions of the pylorus, part of the crab stomach[12]. The pyloric rhythm consists of a triphasic motor pattern in which the pyloric dilator (PD), lateral pyloric (LP) and pyloric

(PY) neurons sequentially fire bursts of action potentials (**Fig. 1a**) to coordinate pyloric contractions[16].

Variability of the output of the pyloric circuit

We examined the variability of the pyloric motor patterns recorded from 69 crabs (**Fig. 1**). For each crab, we recorded 137 cycles (~2 min) of the ongoing pyloric rhythm using extracellular recordings (**Fig. 1a**). For each pyloric cycle, we measured the period and the timing of burst onset and offset for each of the three pyloric phases. By convention, the onset of the PD neuron burst is considered to be the start of each pyloric cycle and the other onset/offset times are measured as the delay from the start of the cycle to the first/last spike of a burst. In this manner, we measured PD neuron burst offset, LP neuron burst onset, LP neuron burst offset, PY neuron burst onset and PY neuron burst offset for each cycle (**Fig. 1a**). The pyloric period was variable from crab to crab; pyloric periods ranged from 0.53–1.44 s, with a coefficient of variation of 18.8% (mean, 0.90 s; s.d., 0.17 s; coefficient of variation is the ratio of the s.d. to the mean, which we report as a percentage; **Fig. 1b**). The pyloric period in each crab was stable from cycle to cycle; the maximum value of the coefficient of variation was 2.6% and the mean coefficient of variation was 1.5% (**Fig. 1b**).

Burst onset and offset delays scaled with pyloric period (**Fig. 1c**). The linear regression lines for each burst onset/offset passed through the origin (y intercept not significantly different from zero, $P > 0.18$ for all burst events), indicating that each delay was proportional to pyloric period. Dividing delay by period gives the phase of each burst event; phase was independent of period (slopes not significantly different from zero, $P > 0.15$ for all burst events; **Fig. 1d**), as implied by the fact that delay scaled with period. The mean phase of each burst event was consistent from crab to crab; PY neuron burst onset showed the highest variability, with an s.d. equal to 0.050 cycles. Burst

[1]Volen Center and Biology Department, Brandeis University, Waltham, Massachusetts, USA. [2]Biological Sciences, University of Missouri at Columbia, Columbia, Missouri, USA. [3]Present address: INSERM UMR 641, Faculté de Médecine-Secteur Nord, Université de la Méditerranée, Marseille, France. Correspondence should be addressed to J.-M.G. (goaillard@univmed.fr).

Figure 1 Variability of pyloric circuit output across crabs. (**a**) Typical extracellular recordings of pyloric neurons. Simultaneous recordings were made from the pyloric dilator nerve (pdn), lateral ventricular nerve (lvn) and pyloric nerve (pyn). The large spikes in the pdn, lvn and pyn recordings are from the PD, LP and PY neurons, respectively. The various measurements of a single cycle (see text) are illustrated by the arrows. (**b**) Histogram showing distribution of mean pyloric period for ganglia from 69 crabs. The smooth curve is a lognormal distribution (used because the data cannot be negative and the histogram is asymmetric) fit to the data. The inset shows the coefficient of variation (CV) of the pyloric period for each crab, plotted versus the mean period for that crab. (**c**) Mean delay versus mean period for each crab. For each neuron burst onset and offset (PD-off, LP-on, LP-off, PY-on and PY-off), the mean delay was plotted versus mean period for each crab. Colors for each event type match those in **a**. In all panels, error bars represent s.d. (but are sometimes smaller than the symbols). Lines are linear fits for each event type. The gray line (largely obscured by PY-off fit line) is the identity line. (**d**) Mean phase versus mean period for each crab. Similar conventions to **c** were used. Inset shows histograms of mean phase for each event type. Smooth curves are normal distributions fit to each dataset. (**e**) Mean PD, LP and PY neuron burst duration versus mean period for each crab, with fits. (**f**) Mean LP neuron ISI versus mean period for each crab, with fit.

durations were proportional to period (y intercept not significantly different from zero, $P > 0.18$ for all bursts; **Fig. 1e**), as burst onsets and offsets both scaled with period.

In each crab, there are two PD neurons and three to five PY neurons, but only one LP neuron. The presence of multiple individual neurons on each pyloric dilator nerve (pdn) and pyloric nerve (pyn) made it difficult to extract spike rates for individual neurons. Because there is a single LP neuron, it was easy to measure the LP neuron interspike interval (ISI) in the burst (**Fig. 1f**). The ISI of LP scaled with pyloric period (y intercept not significantly different from zero, $P = 0.26$). The fact that LP neuron burst duration and ISI both scaled with period implies that the number of LP neuron spikes in the burst does not vary with period, as was the case (data not shown; slope not significantly different from zero, $P = 0.45$).

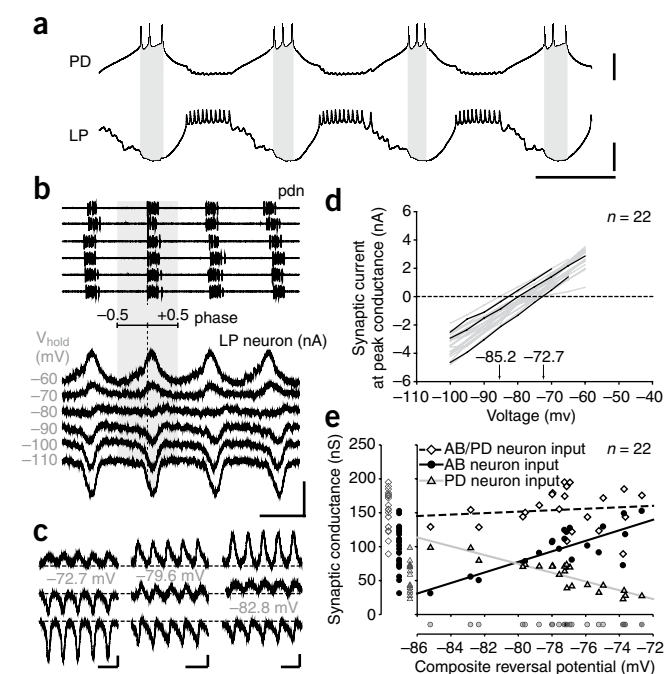**Variability of pacemaker synaptic inputs to the LP neuron**

The firing properties of the crab LP neuron have been extensively studied[17,18], making the LP neuron an ideal choice for studying the relationship between synaptic/cellular properties and circuit function. We first examined the variability of synaptic inputs to the LP neuron. The anterior burster (AB) neuron and the two PD neurons form an electrically-coupled 'pacemaker kernel' that rhythmically inhibits the LP neuron (**Fig. 2a** and **Supplementary Fig. 1**). The AB neuron is glutamatergic and elicits a fast inhibitory postsynaptic potential (IPSP) in the LP neuron with a reversal potential of about −70 mV, whereas the PD neurons are cholinergic and evoke a slower IPSP with a reversal potential of about −90 mV[19,20]. The AB and PD neurons depolarize and fire almost synchronously, and they evoke a composite
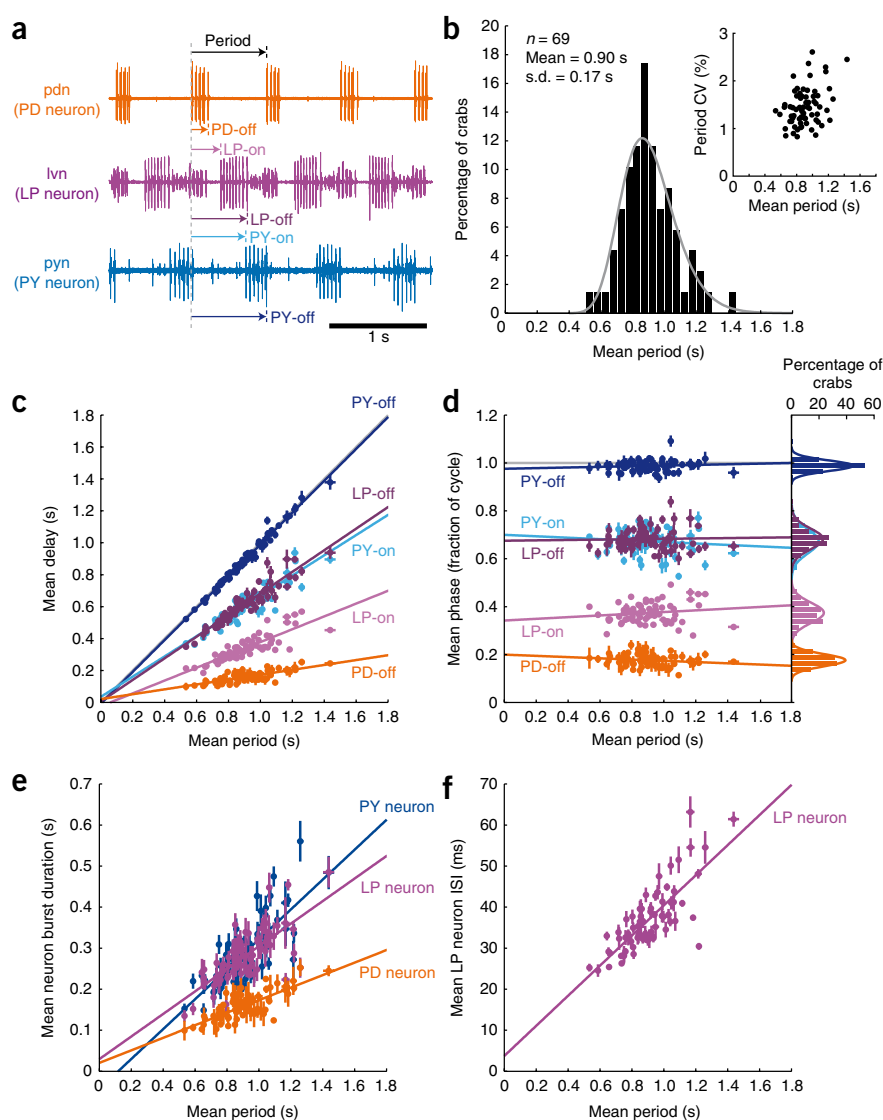
IPSP in the LP neuron with variable contributions from the two classes of presynaptic neurons[19,20]. Because the LP neuron fires on rebound from the synaptic inhibition it receives from the pacemaker kernel (**Fig. 2a** and **Supplementary Fig. 1**), we analyzed the properties of the composite inhibitory postsynaptic current (IPSC) from the AB/PD neurons and then dissociated the composite IPSC into its components from the AB and PD neurons (Online Methods).

To record synaptic currents, we voltage-clamped the LP neuron during the ongoing pyloric rhythm and stepped it to potentials from −120 mV to −60 mV. This changed the pyloric period only slightly, as the pyloric frequency is mainly determined by the intrinsic frequency of the pacemaker kernel, which is the primary driver of oscillatory activity in the pyloric network[21–24]. Simultaneously, we recorded extracellular PD neuron spikes from the pdn (as in **Fig. 1a**) to monitor the phase of the pyloric rhythm. In one typical experiment, the IPSC was outward at −60 mV, was close to reversal at −80 mV and was clearly inward at −90 mV (**Fig. 2b**). This reflects a composite reversal potential between that of the AB neuron synapse (~−70 mV) and that of the PD neuron synapse (~−90 mV).

There was a high degree of variability in the amplitudes and reversal potentials of the IPSCs across preparations. To quantify this, we isolated the synaptic current from other currents by finding the phase

Figure 2 Variability of synaptic inputs to the LP neuron. (**a**) Simultaneous intracellular recordings of the PD and LP neurons. Gray shading shows the pronounced hyperpolarization of LP neuron voltage during PD neuron activity. Vertical scale bars represent −60 to −40 mV and the horizontal scale bar represents 500 ms. (**b**) Synaptic currents recorded in LP neuron during ongoing pyloric activity. ACh, acetylcholine; Glu, glutamate. Extracellular PD neuron recordings (pdn, top traces) were used to align synaptic current traces (bottom traces). Vertical scale bar represents 5 nA and horizontal scale bar represents 500 ms. (**c**) Raw synaptic currents in three preparations with different composite reversal potentials (gray numbers). Traces are from holding potentials of −70, −80 and −90 mV. Black dotted lines represent zero current. Vertical scale bars represent 2 nA and horizontal scale bars represent 1 s. (**d**) Raw *I-V* curves of synaptic current after subtraction of nonsynaptic current (*n* = 22). Black lines correspond to the recordings shown in **c**. Arrows indicate the minimum and maximum values of composite synaptic reversal potential observed across all preparations. (**e**) Plot showing the relationship between maximal synaptic conductance (composite, AB neuron and PD neuron) and composite reversal potential. Data points are projected onto the *x* and *y* axes to show the range of values of the four variables shown.

components, the coefficient of variation of the AB neuron synaptic conductance was 32.5% (mean, 97 nS; s.d., 32 nS) and that of the PD neuron synaptic conductance was 40.5% (mean, 57 nS; s.d., 23 nS).

## Variability of a modulator-activated current in LP neuron

The pacemaker kernel neurons and the LP neuron are modulated by a large number of amines and neuropeptides[12,25] that influence their excitability (**Supplementary Fig. 1**). Among these is the neuropeptide

of the pyloric cycle with the lowest conductance and subtracting this nonsynaptic conductance from the total conductance to get the synaptic conductance (Online Methods). The resulting composite IPSCs had a wide range of reversal potentials (**Fig. 2c**). Reversal potentials were quantified by constructing *I-V* curves of the synaptic current at peak conductance (Online Methods) and ranged from −85.2 mV to −72.7 mV (**Fig. 2d**).

Taking advantage of the difference in reversal potential between the AB neuron– and PD neuron–evoked IPSCs, we decomposed the composite IPSCs into AB neuron– and PD neuron–derived components (Online Methods). Preparations with hyperpolarized composite reversal potentials had relatively large PD neuron–evoked synaptic conductances and small AB neuron–evoked synaptic conductances, whereas those with depolarized composite reversal potentials had large AB neuron–evoked conductances and small PD neuron–evoked conductances (**Fig. 2e**). Consequently, AB neuron– and PD neuron–evoked synaptic conductances showed opposite correlations with the value of the composite reversal potential (slope = 7.8 ± 1.4 nS mV^{-1} and −6.7 ± 0.7 nS mV^{-1}, respectively, $P < 0.001$; ± indicates standard error, here and elsewhere). This was also reflected in the negative correlation between the AB neuron–evoked conductance and the PD neuron–evoked conductance ($r = -0.46$, $P < 0.05$, $n = 22$). The composite synaptic conductance was not correlated with the value of the composite reversal potential (slope = 1.1 ± 2.1 nS mV^{-1}, $P = 0.61$; **Fig. 2e**). All of these quantities had substantial variability (**Fig. 2e**); the coefficient of variation of the composite synaptic conductance was 18.9% (mean, 154 nS; s.d., 29 nS) and the s.d. of the composite reversal potential was 3.1 mV (mean = −77.5 mV). For the individual synaptic

Figure 3 Variability of I_{MI} in the LP neuron. (**a**) Measurement of I_{MI} *I-V* curves. Top, ramp currents recorded in control condition (black line) and in the presence of 10^{-4} M CCAP (gray line). Middle, I_{MI} obtained by subtraction of the control ramp current from the CCAP ramp current (black line). Gray line is the fit obtained using equation 1 (Online Methods). Bottom, fits of I_{MI} obtained from 15 different preparations. Gray circles indicate peak current. (**b**) Variability in amplitude and voltage of peak I_{MI}.
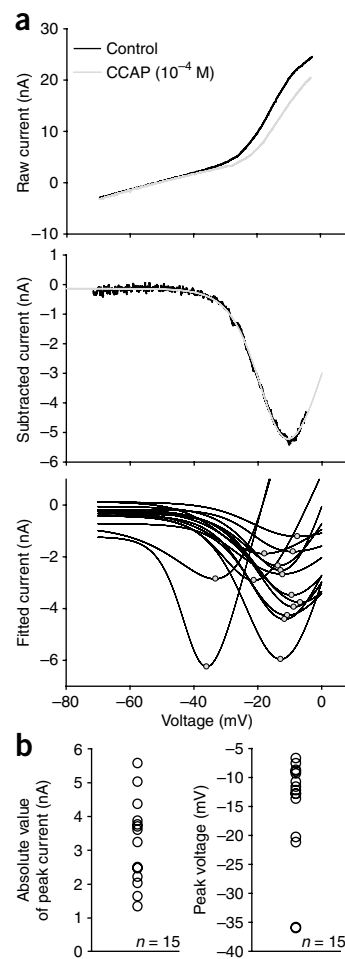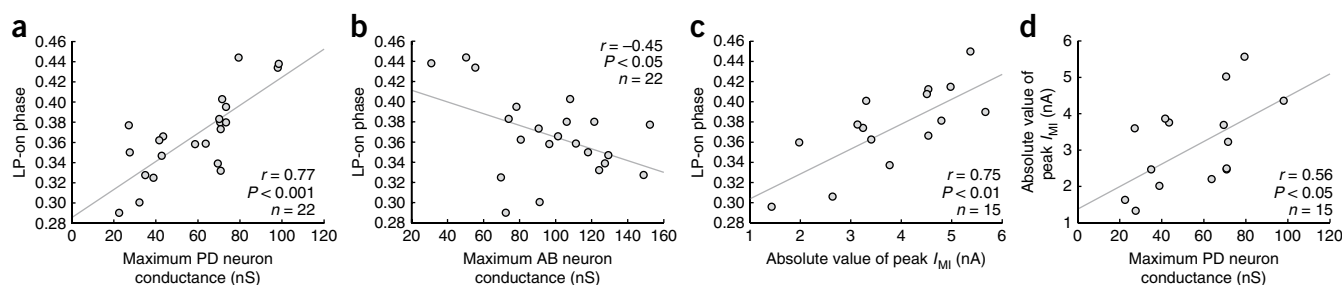
Figure 4 Correlations among synaptic current properties, I_{MI} and LP neuron firing properties. (**a**) LP-on phase was significantly correlated with maximum PD neuron conductance. In all panels, gray line is a linear fit with *x* as the independent variable, *r* is the sample correlation coefficient and the *P* value is from a test of the null hypothesis that the true correlation coefficient is zero (see Online Methods). (**b**) LP-on phase was significantly correlated with maximum AB neuron conductance. (**c**) LP-on phase was significantly correlated with I_{MI} peak current amplitude. (**d**) I_{MI} peak current amplitude was significantly correlated with maximum PD neuron conductance.

crustacean cardioactive peptide (CCAP), which activates a voltage-dependent inward current[26–28] known as the modulator-activated inward current (I_{MI}). CCAP, acting on I_{MI}, strongly modulates the frequency and phasing of the pyloric rhythm[29]. I_{MI} has a bell-shaped steady-state *I-V* curve that makes it sensitive to changes in voltage between −60 mV and −20 mV and it shows little inactivation.
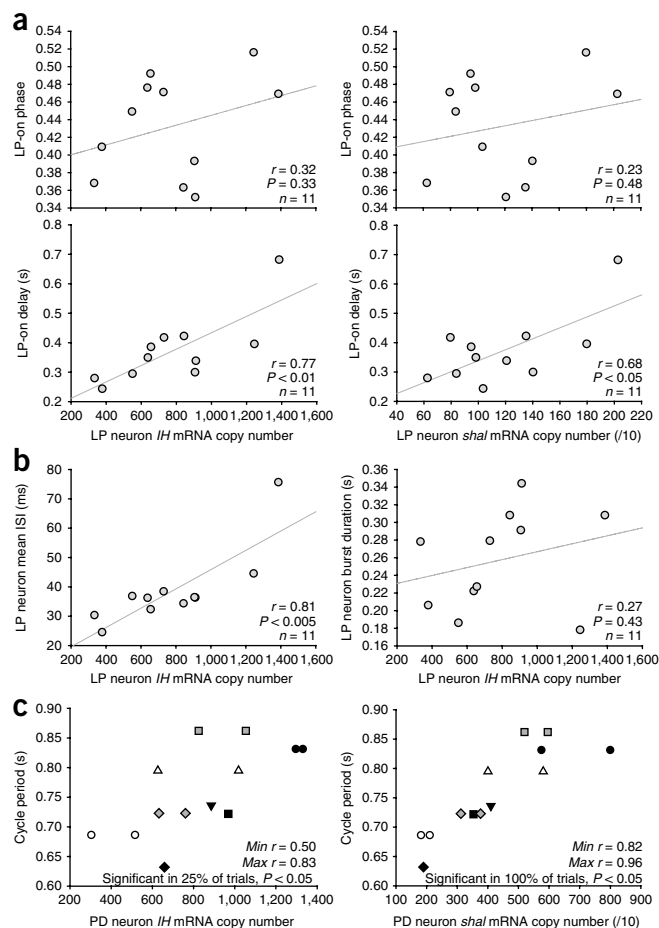
We compared the variability in I_{MI} with the variability of the synaptic currents and looked for correlations between them and between them and the pyloric circuit output. Therefore, we measured I_{MI} in LP neurons by voltage-clamping the neuron and ramping the command potential from −95 to 0 mV (135 mV s^{-1}), both in control saline and while puffing on 10^{-4} M CCAP (**Fig. 3a**). Experiments were carried out in the presence of blockers to eliminate other voltage-gated currents that might have contaminated the measurements of I_{MI} and to eliminate endogenous sources of neuromodulators (Online Methods). I_{MI} was obtained by measuring the current during application of the peptide and then subtracting the current measured before application (**Fig. 3a**). The *I-V* curve obtained was then fit to an equation describing the theoretical steady-state *I-V* curve of I_{MI} (Online Methods). Two parameters were extracted to characterize I_{MI}: the peak current and the voltage at peak current (**Fig. 3a**). These were variable (**Fig. 3b**); the coefficient of variation of the peak current was 38.6% (mean, 3.19 nA; s.d., 1.23 nA) and the s.d. of the voltage at peak current was 7.7 mV (mean, −13.78 mV). There was no significant correlation between the peak current and the voltage at peak current ($r = 0.31$, $P = 0.27$).

Figure 5 Correlations between mRNA expression and network output. (**a**) *IH* and *shal* expression in the LP neuron were significantly correlated with LP-on delay (bottom) but not with LP-on phase (top). In all panels, the gray line is a linear fit with *x* as the independent variable, *r* is the sample correlation coefficient and the *P* value is from a test of the null hypothesis that the true correlation coefficient is zero (see Online Methods). (**b**) *IH* expression in the LP neuron was significantly correlated with mean LP neuron ISI (left) but not with LP neuron burst duration (right). (**c**) *IH* expression in the PD neuron was not significantly correlated with pyloric period (left), but *shal* expression in the PD neuron was significantly correlated (right). Data points with the same symbol are from the same crab (there are two PD neurons per crab). Unpaired symbols are from crabs for which expression levels could only be measured in one PD neuron. Statistical analysis was performed after arbitrarily picking a single PD neuron from each pair (identical symbols, with identical *y* values), leading to 32 replications (see text). Maximum and minimum sample correlation coefficient values obtained across 32 replications are indicated (max *r*, min *r*). Percentage gives the fraction of the 32 replications for which a significant correlation was found ($P < 0.05$).

Correlations among measured quantities in LP neuron

We next looked for correlations between the measured properties of the synaptic currents, I_{MI}, and circuit performance (**Fig. 4**). There was a strong positive correlation between the PD neuron synaptic conductance and the phase of LP neuron burst onset (LP-on phase; **Fig. 4a**). In contrast, we found a negative and weaker correlation between the AB neuron synaptic conductance and the LP-on phase (**Fig. 4b**). The LP-on phase was also positively correlated with the magnitude of the peak I_{MI} (**Fig. 4c**). As expected, we found a positive correlation between the magnitude of the peak I_{MI} and the PD neuron synaptic conductance (**Fig. 4d**).

Table 1 Correlations between synaptic properties, I_{MI} properties, channel expression and firing properties in the LP and PD neurons

Correlation	r	n	P
Firing properties (LP neuron)			
Period versus LP-on delay	0.85	69	<0.001
Period versus mean LP neuron ISI	0.78	69	<0.001
Period versus LP neuron burst duration	0.73	69	<0.001
LP-on delay versus mean LP neuron ISI	0.75	69	<0.001
Synaptic properties (LP neuron)			
E_{rev} versus Max gAB	0.77	22	<0.001
E_{rev} versus Max gPD	−0.90	22	<0.001
Max gAB versus Max gPD	−0.46	22	<0.05
Max gPD versus phase of Max gABPD	0.57	22	<0.01
Max gABPD versus phase of max gABPD	0.43	22	<0.05
Synaptic versus firing (LP neuron)			
Max gAB versus LP-on phase	−0.45	22	<0.05
Max gPD versus LP-on phase	0.77	22	<0.001
gAB-gPD versus LP-on phase	−0.68	22	<0.001
Phase of Max gABPD versus LP-on phase	0.62	22	<0.005
Synaptic versus I_{MI} (LP neuron)			
Max gPD versus peak I_{MI}	0.56	15	<0.05
Phase of Max gABPD versus peak I_{MI}	0.64	15	<0.05
I_{MI} versus firing (LP neuron)			
Peak I_{MI} versus LP-on phase	0.75	15	<0.005
Channel expression versus firing (LP neuron)			
IH versus mean LP neuron ISI	0.81	11	<0.005
IH versus LP-on delay	0.77	11	<0.05
IH versus pyloric period	0.69	11	<0.05
shal versus mean LP neuron ISI	0.75	11	<0.01
shal versus LP-on delay	0.68	11	<0.05
shal versus pyloric period	0.63	11	<0.05
shaw verus mean LP neuron ISI	0.69	10	<0.05
shaw versus LP-on delay	0.63	10	<0.05
shab versus mean LP neuron ISI	0.66	10	<0.05
Channel expression versus firing (PD neuron)			
shal versus pyloric period (all cells included)	0.87	13	<0.001

E_{rev}, composite synaptic reversal potential; peak I_{MI}, absolute value of peak I_{MI} current amplitude; phase of max gABPD, phase of maximum composite synaptic conductance.

Because the LP and PY neurons fire on rebound from inhibition, the dependence of their firing phase on the hyperpolarization-activated inward current (I_H) and the transient outward current (I_A) has been extensively studied[10,14,15,30]. Overexpression of the mRNA encoding the channel responsible for I_A causes an increase in I_H[10,30], and expression of the mRNAs that code for the channels responsible for I_H and I_A is highly correlated in individual LP neurons of *C. borealis* across crabs[7,11]. Consequently, we asked how mRNA expression of these channel genes correlated with circuit output. In 11 experiments, we measured the mRNA levels of six channel subunits after physiological recordings: *shal* (I_A), *IH* (I_H), *shab* (a delayed-rectifier potassium current), *shaw* (a different delayed-rectifier potassium current), *para* (the fast sodium channel) and *BKKCa* (a calcium-dependent potassium current)[11] (each mRNA codes for a subunit of the indicated channel). In the LP neuron, there was no significant correlation between *IH* copy number and LP-on phase ($r = 0.32$, $P = 0.33$, $n = 11$; **Fig. 5a**) and no significant correlation between *shal* copy number and LP-on phase ($r = 0.23$, $P = 0.48$, $n = 11$; **Fig. 5a**), but the copy number of both genes was significantly correlated with LP-on delay (*IH*: $r = 0.77$, $P < 0.01$, $n = 11$; *shal*: $r = 0.68$, $P < 0.05$, $n = 11$; **Fig. 5a**). The expression levels of these two genes were also significantly correlated with LP neuron mean ISI (*IH*: $r = 0.81$, $P < 0.005$, $n = 11$; **Fig. 5b**; *shal*: $r = 0.75$, $P < 0.01$, $n = 11$; data not shown) and with pyloric period (*IH*: $r = 0.69$,

$P < 0.05$, $n = 11$; *shal*: $r = 0.63$, $P < 0.05$, $n = 11$; data not shown), but failed to show a significant correlation with LP neuron burst duration (*IH*: $r = 0.27$, $P = 0.43$, $n = 11$; **Fig. 5b**; *shal*: $r = 0.16$, $P = 0.637$, $n = 11$; data not shown).

Pyloric period was strongly correlated with LP-on delay, LP neuron mean ISI and LP neuron burst duration (**Fig. 1** and **Table 1**). In addition, the expression levels of *IH*, *shal*, *shaw* and *shab* are strongly correlated with one another in the LP neuron[7,11]. Therefore, we looked for correlations between the level of expression of these channels and LP neuron firing properties. The expression of the *shaw* channel had a significant correlation with LP-on delay ($r = 0.63$, $P < 0.05$, $n = 10$; data not shown) and LP mean ISI ($r = 0.69$, $P < 0.05$, $n = 10$; data not shown), but not with pyloric period ($r = 0.54$, $P = 0.111$, $n = 10$; data not shown) or LP neuron burst duration ($r = 0.06$, $P = 0.878$, $n = 10$; data not shown). *Shab* expression was significantly correlated with LP neuron mean ISI ($r = 0.66$, $P < 0.05$, $n = 10$; data not shown), but not with other firing parameters, such as pyloric period ($r = 0.52$, $P = 0.126$, $n = 10$; data not shown), LP-on delay ($r = 0.57$, $P = 0.0824$, $n = 10$; data not shown) and LP neuron burst duration ($r = 0.23$, $P = 0.523$, $n = 10$; data not shown).

shal expression level in PD neuron scales with pyloric period

The PD neurons are part of the pacemaker kernel. Because I_H and I_A are important for burst properties in many systems[9,31], we asked whether the expression of *IH* and *shal* in the PD neurons might be correlated with the pyloric period.

The two PD neurons from the same crab showed very similar levels of expression for both *IH* and *shal*[7]. This similarity becomes a problem when studying correlations between a circuit property (pyloric period) and the expression levels in two PD cells from the same preparation. The PD neurons were from eight crabs, five with data from two PD neurons and three with data from one PD neuron. When calculating correlations, we arbitrarily picked a single PD neuron from those with measurements for both. We repeated this process 32 times, once for each possible combination. Thus, each correlation was calculated from data from eight PD neurons, one from each preparation.

IH expression was significantly correlated with pyloric period for only 25% of the 32 combinations ($0.50 \leq r \leq 0.83$, $\alpha = 0.05$, $n = 8$; **Fig. 5c**), whereas *shal* levels were significantly correlated with pyloric period for all combinations ($0.82 \leq r \leq 0.96$, $\alpha = 0.05$, $n = 8$; **Fig. 5c**). In contrast, *BKKCa* expression did not show a significant correlation with pyloric period, even when all PD neurons (including paired PD neurons) were included ($r = 0.25$, $P = 0.41$, $n = 13$). *BKKCa* expression was nonetheless strongly correlated with *shal* expression ($r = 0.92$, $P < 0.01$, $n = 8$). In summary, only the *shal* expression level in the PD neuron was significantly correlated with pyloric period.

DISCUSSION

The crabs that we used had spent years foraging for food in the cold waters of the Atlantic Ocean before being trapped by fishermen. As such, they were all successful survivors of the vagaries of their sometimes inhospitable natural environment and, by definition, their nervous systems were good enough for them to feed, grow and molt. Consequently, the variability we found here is likely to be a representative sample of the natural population, with its disparate genetic make-ups and life histories. Differences in both genetic make-up and life history could lead to variability in synaptic strengths, voltage-gated channel densities, and baseline neuromodulator/hormonal concentrations.

Previous work on voltage-dependent currents and the expression of the mRNAs encoding the channel proteins responsible for them in crabs showed 2–4-fold animal-to-animal variability in the same

identified neurons[2,6,7], and similarly variable levels of conductances in neurons of the same type in genetically identical mice[5,8]. We found several-fold animal-to-animal variability of the conductances of identified synapses, similar to that seen at identified synapses in the leech heartbeat system[32,33]. In addition, the I_{MI} modulatory conductance was highly variable across crabs, with an almost sixfold range in its amplitude and considerable variation in its voltage dependence.

We found 2–3-fold variability in pyloric period across crabs, but also found that many aspects of pyloric output scaled with period, and are therefore phase constant (**Fig. 1**). These results are consistent with similar results from studies of the American lobster, *Homarus americanus*[34]. We found relatively little variability in the pyloric rhythm from cycle to cycle (**Fig. 1b–e**). This contrasts with feeding behavior in *Aplysia californica,* which exhibits substantial cycle-to-cycle variability, and where the question of how good is good enough has been raised in a different context[35].

When studying animal-to-animal variability, it is essential to establish that one is not simply observing variability caused by measurement error. Two observations indicate that measurement error cannot account for most of the variability observed here. First, the mRNA levels measured in the electrically coupled PD neurons from a single crab showed much less variation than that found in PD neurons from different crabs[7]. Second, the strong correlations presented here and previously[7,11] argue strongly that much of the variability is true animal-to-animal variation.

Thus, there are two remaining explanations of the several-fold variability in neuronal and network parameters that have been measured here and previously[5,7,11,32,33]. The variability could occur because the value of a given parameter is not critical for the performance of the system. For example, once an inhibitory synaptic input to an oscillatory neuron is strong enough, increasing it further may have no effect on the oscillator's behavior[23,35]. Alternatively, the variability could be accompanied by compensatory covariation of other parameters, which would induce correlations among different parameters. To understand how important a given parameter is for system function, one must know which of these possibilities accounts for the measured variation across individuals. The answer to this question has important implications for understanding the mechanisms by which synaptic strength and intrinsic properties are regulated.

Here, we related circuit performance to multiple underlying parameters by looking at variability and correlations among them. More commonly, attempts to connect an intrinsic or synaptic current to a neuron's firing have experimentally perturbed a single parameter at a time. For example, the dynamic clamp is often used to alter the parameters of a single current to determine how the firing properties of a neuron or a network are affected by that current[35–37]. This is similar to conventional sensitivity analysis in theoretical studies[18]. These start with an individual and look at the effects of changing a single parameter on system behavior. In contrast, our approach starts with a natural population and asks whether there are correlations among any of the parameters and system behaviors. To the best of our knowledge, something similar has been done only once before and was limited to examining the relationship between I_A current density, the mRNAs that code for I_A channel subunits, and spontaneous spike rate; the last of which was found to be negatively correlated with the first two in substantia nigra dopaminergic neurons[8].

We found several correlations among intrinsic, synaptic and functional properties in both PD and LP neurons (**Supplementary Fig. 2**). The strongest correlation between PD neuron parameters and circuit output was between *shal* expression and pyloric period (**Supplementary Fig. 2**), which makes intuitive sense because

I_A acts to delay burst onset[15,38]. In the LP neuron, the expression levels of *IH*, *shal*, *shab* and *shaw* formed a nested 'Venn diagram' of correlations with different network properties (**Supplementary Fig. 2**). All were correlated with one another and all were correlated with the ISI of the LP neuron. *IH*, *shab* and *shaw* expression were correlated with LP–on delay. *IH* and *shal* were strongly correlated with the pyloric period. Thus, both the PD neuron's and the LP neuron's *shal* expression were correlated with the overall period.

There was a strong correlation between the strength of the PD neuron–evoked synaptic current and the amplitude of I_{MI}, and high values of these imply a later phase of LP neuron burst onset (**Supplementary Fig. 2**). A similar relationship between the strength of the slow IPSP evoked by the PD neuron and the phase of follower neuron firing was seen previously when the strength of the synapse was varied[13]. In this example, single parameter manipulations and the examination of correlations across animals give congruent results. Both results make sense because the synapses from the PD neurons are slower and longer-lasting than those from the AB neuron[19,20], so they are more important for determining the burst onset in follower neurons. In contrast with our results, others have reported a negative correlation between IPSP amplitude and LP-on phase, for the IPSPs from both the AB and PD neurons onto the LP neuron, in the spiny lobster *Panulirus interruptus*[39]. The apparent contradiction between our findings and theirs could result from the difference in species or in experimental design.

At first glance, the strong positive correlation between I_{MI} and LP-on phase is counterintuitive, as one would expect that increasing I_{MI} would advance LP neuron onset phase by making LP neuron more excitable[21,27,28]. However, because there appear to be strong pressures for the pyloric rhythm to remain phase constant (**Fig. 1**), it is possible that the strength of the PD neuron–to–LP neuron synapse and I_{MI} are coordinately regulated so that the increase in I_{MI} partially, but incompletely, compensates for the effects of increasing the strength of the PD neuron–to–LP neuron synapse.

All of these interactions can be summarized as a network of correlations, in which various intrinsic and synaptic properties of the pyloric circuit are correlated with one another and with particular circuit output properties (**Supplementary Fig. 2**). Notably, our data provide evidence that synaptic inputs from different neurons might be regulated in a coordinated manner to reach a specific functional output: AB neuron–to–LP neuron and PD neuron–to–LP neuron synaptic conductances were significantly negatively correlated, such that the total conductance was held approximately constant (**Fig. 2e**).

Expression of the LP neuron's channel mRNAs seemed to correlate more strongly with the LP neuron's single-cell firing properties than with more circuit-level properties. In particular, four mRNA species correlated with LP neuron ISI, three correlated with LP-on delay and only two with pyloric period. This may reflect the fact that ISI during the burst is mainly set by LP neuron's intrinsic properties, the delay is set partly by intrinsic properties and partly by the properties of other cells and synapses in the circuit, and the period is even more dependent on factors extrinsic to the LP neuron. In addition, it is noteworthy that the intrinsic currents in the LP neuron were correlated with quantities measured in units of time (ISI, LP-on delay and period), but the synaptic and I_{MI} currents were correlated with the phase of LP-on delay (that is, delay normalized by period). It is interesting to speculate that different regulatory schemes might be required for the homeostatic control of delays versus phases. According to this hypothesis, *IH*, *shal*, *shab* and *shaw* would belong to one regulatory subnetwork, whereas the synaptic conductances and the I_{MI} current would belong to a different one.

Despite the apparent logic of the relationships that we observed (**Supplementary Fig. 2**), the existence of correlations does not imply that these correlations are necessary for the function of the network, as some correlations among ion channels or receptors could be a consequence of developmental or transcriptional processing, but may not be strictly required for the production of dynamics. This possibility was underscored by a recent computational study of a population of LP neuron models, which failed to find strong correlations between LP neuron parameters, even though the models were constrained to behave like biological LP cells[18].

Studies on non-neuronal systems have shown that genetically identical cells or animals show substantial variability in many underlying cellular parameters and that variable solutions to the production of similar phenotypes are an important substrate for evolutionary selection[40,41]. Although it is tempting to think that brain circuits are optimally designed, a large body of work suggests that there are many 'good enough' solutions consistent with the normal behavior of healthy animals in their usual environments. These solutions will be accompanied by variable sets of network parameters and the challenge is to discover new experimental strategies, such as the multidimensional measurements used here, that can assess which neuronal and circuit elements are variable, but functionally critical, and which are only loosely controlled, as they are less essential for the animal's behavior.

METHODS

Methods and any associated references are available in the online version of the paper at http://www.nature.com/natureneuroscience/.

Note: Supplementary information is available on the Nature Neuroscience website.

1. Prinz, A.A., Bucher, D. & Marder, E. Similar network activity from disparate circuit parameters. *Nat. Neurosci.* **7**, 1345–1352 (2004).
2. Goldman, M.S., Golowasch, J., Marder, E. & Abbott, L.F. Global structure, robustness and modulation of neuronal models. *J. Neurosci.* **21**, 5229–5238 (2001).
3. Achard, P. & De Schutter, E. Complex parameter landscape for a complex neuron model. *PLoS Comput. Biol.* **2**, e94 (2006).
4. Marder, E. & Goaillard, J.M. Variability, compensation and homeostasis in neuron and network function. *Nat. Rev. Neurosci.* **7**, 563–574 (2006).
5. Swensen, A.M. & Bean, B.P. Robustness of burst firing in dissociated purkinje neurons with acute or long-term reductions in sodium conductance. *J. Neurosci.* **25**, 3509–3520 (2005).
6. Golowasch, J., Abbott, L.F. & Marder, E. Activity-dependent regulation of potassium currents in an identified neuron of the stomatogastric ganglion of the crab *Cancer borealis. J. Neurosci.* **19**, RC33 (1999).
7. Schulz, D.J., Goaillard, J.M. & Marder, E. Variable channel expression in identified single and electrically coupled neurons in different animals. *Nat. Neurosci.* **9**, 356–362 (2006).
8. Liss, B. *et al.* Tuning pacemaker frequency of individual dopaminergic neurons by Kv4.3L and KChip3.1 transcription. *EMBO J.* **20**, 5715–5724 (2001).
9. Liss, B. & Roeper, J. Correlating function and gene expression of individual basal ganglia neurons. *Trends Neurosci.* **27**, 475–481 (2004).
10. MacLean, J.N. *et al.* Activity-independent coregulation of I_A and I_h in rhythmically active neurons. *J. Neurophysiol.* **94**, 3601–3617 (2005).
11. Schulz, D.J., Goaillard, J.M. & Marder, E.E. Quantitative expression profiling of identified neurons reveals cell-specific constraints on highly variable levels of gene expression. *Proc. Natl. Acad. Sci. USA* **104**, 13187–13191 (2007).
12. Marder, E. & Bucher, D. Understanding circuit dynamics using the stomatogastric nervous system of lobsters and crabs. *Annu. Rev. Physiol.* **69**, 291–316 (2007).
13. Eisen, J.S. & Marder, E. A mechanism for production of phase shifts in a pattern generator. *J. Neurophysiol.* **51**, 1375–1393 (1984).
14. Harris-Warrick, R.M., Coniglio, L.M., Barazangi, N., Guckenheimer, J. & Gueron, S. Dopamine modulation of transient potassium current evokes phase shifts in a central pattern generator network. *J. Neurosci.* **15**, 342–358 (1995).
15. Harris-Warrick, R.M., Coniglio, L.M., Levini, R.M., Gueron, S. & Guckenheimer, J. Dopamine modulation of two subthreshold currents produces phase shifts in activity of an identified motoneuron. *J. Neurophysiol.* **74**, 1404–1420 (1995).
16. Thuma, J.B., Harness, P.I., Koehnle, T.J., Morris, L.G. & Hooper, S.L. Muscle anatomy is a primary determinant of muscle relaxation dynamics in the lobster (*Panulirus interruptus*) stomatogastric system. *J. Comp. Physiol. A Neuroethol. Sens. Neural Behav. Physiol.* **193**, 1101–1113 (2007).
17. Golowasch, J. & Marder, E. Ionic currents of the lateral pyloric neuron of the stomatogastric ganglion of the crab. *J. Neurophysiol.* **67**, 318–331 (1992).
18. Taylor, A.L., Goaillard, J.M. & Marder, E. How multiple conductances determine electrophysiological properties in a multicompartmental model. *J. Neurosci.* **29**, 5573–5586 (2009).
19. Eisen, J.S. & Marder, E. Mechanisms underlying pattern generation in lobster stomatogastric ganglion as determined by selective inactivation of identified neurons. III. Synaptic connections of electrically coupled pyloric neurons. *J. Neurophysiol.* **48**, 1392–1415 (1982).
20. Marder, E. & Eisen, J.S. Transmitter identification of pyloric neurons: electrically coupled neurons use different neurotransmitters. *J. Neurophysiol.* **51**, 1345–1361 (1984).
21. Hooper, S.L. & Marder, E. Modulation of the lobster pyloric rhythm by the peptide proctolin. *J. Neurosci.* **7**, 2097–2112 (1987).
22. Miller, J.P. Pyloric mechanisms. in *The Crustacean Stomatogastric System* (eds. Selverston, A.I. & Moulins, M.) 109–145 (Springer-Verlag, Berlin, 1987).
23. Thirumalai, V., Prinz, A.A., Johnson, C.D. & Marder, E. Red pigment concentrating hormone strongly enhances the strength of the feedback to the pyloric rhythm oscillator but has little effect on pyloric rhythm period. *J. Neurophysiol.* **95**, 1762–1770 (2006).
24. Nadim, F., Manor, Y., Kopell, N. & Marder, E. Synaptic depression creates a switch that controls the frequency of an oscillatory circuit. *Proc. Natl. Acad. Sci. USA* **96**, 8206–8211 (1999).
25. Nusbaum, M.P., Blitz, D.M., Swensen, A.M., Wood, D. & Marder, E. The roles of co-transmission in neural network modulation. *Trends Neurosci.* **24**, 146–154 (2001).
26. Swensen, A.M. & Marder, E. Multiple peptides converge to activate the same voltage-dependent current in a central pattern-generating circuit. *J. Neurosci.* **20**, 6752–6759 (2000).
27. Swensen, A.M. & Marder, E. Modulators with convergent cellular actions elicit distinct circuit outputs. *J. Neurosci.* **21**, 4050–4058 (2001).
28. Golowasch, J. & Marder, E. Proctolin activates an inward current whose voltage dependence is modified by extracellular Ca2+. *J. Neurosci.* **12**, 810–817 (1992).
29. Weimann, J.M. *et al.* Modulation of oscillator interactions in the crab stomatogastric ganglion by crustacean cardioactive peptide. *J. Neurosci.* **17**, 1748–1760 (1997).
30. MacLean, J.N., Zhang, Y., Johnson, B.R. & Harris-Warrick, R.M. Activity-independent homeostasis in rhythmically active neurons. *Neuron* **37**, 109–120 (2003).
31. Lüthi, A. & McCormick, D.A. H-current: properties of a neuronal and network pacemaker. *Neuron* **21**, 9–12 (1998).
32. Norris, B.J., Weaver, A.L., Wenning, A., Garcia, P.S. & Calabrese, R.L. A central pattern generator producing alternative outputs: pattern, strength and dynamics of premotor synaptic input to leech heart motor neurons. *J. Neurophysiol.* **98**, 2992–3005 (2007).
33. Norris, B.J., Weaver, A.L., Wenning, A., Garcia, P.S. & Calabrese, R.L. A central pattern generator producing alternative outputs: phase relations of leech heart motor neurons with respect to premotor synaptic input. *J. Neurophysiol.* **98**, 2983–2991 (2007).
34. Bucher, D., Prinz, A.A. & Marder, E. Animal-to-animal variability in motor pattern production in adults and during growth. *J. Neurosci.* **25**, 1611–1619 (2005).
35. Prinz, A.A., Thirumalai, V. & Marder, E. The functional consequences of changes in the strength and duration of synaptic inputs to oscillatory neurons. *J. Neurosci.* **23**, 943–954 (2003).
36. van Welie, I., van Hooft, J.A. & Wadman, W.J. Homeostatic scaling of neuronal excitability by synaptic modulation of somatic hyperpolarization-activated I_h channels. *Proc. Natl. Acad. Sci. USA* **101**, 5123–5128 (2004).
37. Lien, C.C. & Jonas, P. Kv3 potassium conductance is necessary and kinetically optimized for high-frequency action potential generation in hippocampal interneurons. *J. Neurosci.* **23**, 2058–2068 (2003).
38. Tierney, A.J. & Harris-Warrick, R.M. Physiological role of the transient potassium current in the pyloric circuit of the lobster stomatogastric ganglion. *J. Neurophysiol.* **67**, 599–609 (1992).
39. Rabbah, P. & Nadim, F. Distinct synaptic dynamics of heterogeneous pacemaker neurons in an oscillatory network. *J. Neurophysiol.* **97**, 2239–2253 (2007).
40. Greenspan, R.J. The flexible genome. *Nat. Rev. Genet.* **2**, 383–387 (2001).
41. Chouard, T. Darwin 200: beneath the surface. *Nature* **456**, 300–303 (2008).

ONLINE METHODS

Adult *Cancer borealis* crabs were obtained from Commercial Lobster and maintained in artificial seawater until used. Crabs were anesthetized by keeping them on ice for 30 min before dissection. The complete stomatogastric nervous system, consisting of the paired commisural ganglia, the esophageal ganglion, the STG and some of the motor nerves, was dissected out of the crab and pinned out in a Sylgard-coated (Dow Corning) dish containing chilled (9–13 °C) saline. The physiological saline solution consisted of 440 mM NaCl, 11 mM KCl, 13 mM CaCl$_2$, 26 mM MgCl$_2$, 11 mM Trizma and 5 mM maleic acid, pH 7.45.

Quantitative single-cell reverse transcription PCR. Data on the expression levels of *IH*, *shal*, *shaw* and *shab* mRNA presented here (**Fig. 5** and **Table 1**) were described previously[11]. Physiological analysis of these experiments and correlation of mRNA levels with firing pattern were performed specifically for the current study.

Electrophysiological recordings. For electrophysiological recordings, the STG was desheathed and petroleum jelly wells were placed on the motor nerves. Extracellular recordings from the nerves were made by placing stainless steel pin electrodes in the wells. Signals were amplified and filtered using a differential amplifier (A-M Systems). Intracellular recordings from the STG somata were made using 20–40 MΩ glass microelectrodes filled with 0.6 M K$_2$SO$_4$ and 20 mM KCl with an Axoclamp 2A amplifier (Molecular Devices). Pyloric motor neurons were identified using standard procedures for *C. borealis*[42,43]. During recording, the preparation was continuously superfused with chilled (9–13 °C) physiological saline.

For control recordings of the ongoing pyloric rhythm (**Fig. 1**), 137 cycles (~2 min) of the pyloric rhythm were recorded from each crab. All stomatogastric nervous systems used for these recordings had two intact superior esophageal nerves, but they varied in the number of intact inferior esophageal nerves (ions). Of the 69 control crabs, 47 had two ions (mean period = 0.88 ± 0.02, s.d. = 0.16 ± 0.03), 13 had one ion (mean period = 0.97 ± 0.06, s.d. = 0.21 ± 0.04) and 12 had no ions (mean period = 0.95 ± 0.04, s.d. = 0.14 ± 0.03). These differences in mean period, although suggestive, did not achieve statistical significance, using either one-way ANOVA ($P = 0.15$) or the Kruskal-Wallis test ($P = 0.10$), and the standard deviations indicate that there was substantial overlap between the three populations. Control recordings were used only if there was no visible nonstationarity (a slow trend) or gastric modulation in the sequence of 137 cycles, either in the period or the delays to burst onset/offset. We took the first/last spike of each burst on the pdn recording (from either PD neuron) as the PD neuron burst onset/offset and used the first/last spike of each burst on the pyn recording (from any PY neuron) as the PY neuron burst onset/offset. Because the timing of the last spike during the LP neuron burst is far more variable than the timing of the other spikes, the last spike was not included in calculations of mean LP neuron ISI. The ongoing pyloric rhythm (**Figs. 1, 4** and **5**) was recorded extracellularly before any neuron was impaled with microelectrodes.

Synaptic current recordings and analysis. To record synaptic currents, we voltage-clamped the LP neuron and stepped them to hyperpolarized potentials ranging from −60 to −120 mV during the ongoing pyloric rhythm. Extracellular PD neuron spikes were recorded from the pdn to monitor the ongoing pyloric rhythm (**Fig. 2b**). Synaptic currents were measured in control saline to preserve spontaneous pyloric activity and they were always measured before the PD cells were impaled. For larger hyperpolarizations, a noticeable I_H developed after several pyloric cycles. I_H activates quite slowly in *C. borealis*; the smallest time constant over the range of voltages used is >5 s[17,44]. To minimize contamination of synaptic current measurements by I_H, we analyzed only the first three cycles after the start of the hyperpolarizing step. Each time sample of each synaptic current recording was assigned a corresponding pyloric phase using the recording of PD neuron spikes (**Supplementary Fig. 3**). By convention, the onset of the PD neuron burst was defined as having a phase of zero (**Fig. 2b**). Phase was then binned into 100 bins and all current samples in the same phase bin were averaged together. We then computed the *I-V* curve for each phase bin (**Supplementary Fig. 3**) and fit a line to each *I-V* curve (**Supplementary Fig. 3**). For these fits, we only used voltages between −95 and −75 mV, to prevent contamination by voltage-activated currents. The slope of each of these lines gives the total conductance

for that phase bin. We assumed that the minimum conductance represented the nonsynaptic conductance and subtracted out the nonsynaptic *I-V* curve to determine the synaptic current at each phase and voltage (**Supplementary Fig. 3**). If there is baseline synaptic release even at the minimum-conductance point, then our measure would be the synaptic conductance that varies over a pyloric cycle. A linear fit of the synaptic *I-V* curve was performed at each phase (**Supplementary Fig. 3**). The slope of each line gives the total conductance of the synaptic input at that phase and the *x* intercept (the voltage at which the current is zero) gives the composite reversal potential. These were then plotted versus the pyloric phase (**Supplementary Fig. 3**). These plots were used to determine the maximum composite synaptic conductance (max gABPD in **Table 1** and **Supplementary Fig. 3**), the phase at which this maximum occurred (phase of max gABPD in **Table 1**) and the composite reversal potential at this phase (E$_{rev}$ in **Table 1** and **Supplementary Fig. 3**; see also **Fig. 2** for data on all of these quantities).

The synaptic conductance at each phase is the sum of the synaptic conductance from the AB cell (glutamatergic) and from the PD cells (cholinergic)[20]. Because the synaptic input from the AB cell reverses at −70 mV and the input from the PD cells reverses at −90 mV[20], the synaptic *I-V* curve at each phase can be used to estimate both the AB and PD neuron conductance at that phase. This was done using a non-negative least-squares regression to the synaptic *I-V* curve for voltages from −95 to −75 mV. This regression determined the AB and PD neuron conductances that provided the best fit to the synaptic *I-V* curve, subject to the constraint that conductances be non-negative. Because of uncertainty about the precise reversal potentials, several combinations of values for AB and PD neuron reversal potentials were used (−70/−90, −70/−85, −65/−85). Although modifying reversal potentials changed somewhat the relative contribution of the AB and PD neurons to the synaptic input, the main results of our study (weak correlation between AB neuron conductance and LP-on phase, strong correlation between PD neuron conductance and LP-on phase and strong correlation between PD neuron conductance and I_{MI} current; **Fig. 4**) were insensitive to these changes. Therefore, we used the values of −70 and −90 mV in results shown here. It is reassuring that the PD neuron synaptic component extracted in this way generally outlasted that of the AB neuron (**Supplementary Fig. 3**; note that the PD neuron component was generally larger for phases from +0.25 to +0.5), consistent with the PD neuron synapse being slower than that of the AB neuron[20,39].

I_{MI} current recordings and analysis. For I_{MI} measurements, voltage-activated and synaptic currents were blocked by adding 0.1 μM tetrodotoxin (Alomone Laboratories), 10 μM picrotoxin (Sigma; picrotoxin blocks glutamatergic transmission in *C. borealis*) and 10 mM tetraethylammonium chloride (Sigma) to the bath saline. I_{MI} was elicited using long-lasting puff applications (10–20 s) of CCAP (Bachem) at saturating concentration (100 μM) using a Picospritzer (General Valve). Although I_{MI} is activated by many peptides[26,27], CCAP was used because it generally produces larger responses in the LP neuron than other agonists. CCAP acts hormonally on the STG[12], but all of the preparations studied here were deprived of endogenous CCAP for approximately 2 h before the I_{MI} current was measured, presumably minimizing any variability in the recorded current caused by variability in receptor desensitization. Furthermore, most nonhormonal neuromodulators released onto STG neurons are released from the terminals of axonal projections from other ganglia and all or most of this release is blocked by the presence of tetrodotoxin, which blocks spikes in these axons[12]. Variability in the state of second messenger pathways mediating the CCAP response may be reflected in our measurements. I_{MI} was measured by applying voltage ramps (−95 to 0 mV, 135 mV s^{-1}) to the cell in control saline and during CCAP application and subtracting control ramp current from CCAP ramp current (**Fig. 3a**). I_{MI} *I-V* curves were fit by the equation

$$i(v) = i_0 + \overline{g}\,\frac{1}{1+\exp\dfrac{-(v-v_{half})}{s}}(v-e_{rev}) \qquad (1)$$

where i_0 is basal current, $\overline{g}$ is the maximal conductance of the current, v is voltage, v_{half} is half-activation voltage, s scales the voltage-sensitivity of activation and e_{rev} is the reversal potential of the current.

Data acquisition and analysis. Data were acquired using a Digidata 1200 data acquisition board (Axon Instruments) and subsequently analyzed in Clampfit

(version 9, Axon Instruments), Matlab (version R2006b, Mathworks) and Spike2 (version 4, Cambridge Electronic Design). Analyzed data were plotted using SigmaPlot (version 10, Systat Software) and statistical tests were performed in SigmaStat (version 3.5, Systat Software). Sample correlation coefficients were calculated in the usual way, tested for significance by *t* test and considered to be significant for *P* values less than 0.05. Final figure composition was done in Adobe Illustrator 10 (Adobe Systems).

42. Hooper, S.L. *et al.* The innervation of the pyloric region of the crab, *Cancer borealis*: homologous muscles in decapod species are differently innervated. *J. Comp. Physiol. [A]* **159**, 227–240 (1986).
43. Weimann, J.M., Meyrand, P. & Marder, E. Neurons that form multiple pattern generators: identification and multiple activity patterns of gastric/pyloric neurons in the crab stomatogastric system. *J. Neurophysiol.* **65**, 111–122 (1991).
44. Buchholtz, F., Golowasch, J., Epstein, I.R. & Marder, E. Mathematical model of an identified stomatogastric ganglion neuron. *J. Neurophysiol.* **67**, 332–340 (1992).